16th World Conference on Earthquake, 16WCEE 2017

Santiago Chile, January 9th to 13th 2017

Paper N° 3473

Registration Code: S-H1463009060

Experiment and analytical modeling of high-stiffness viscoelastic material with reduced temperature sensitivity

Tomokazu Takada[1], Kaoru Yasui[2], Takeshi Nomura[3] , Kazuhiko Kasai[4] and Hisao Yamazaki[5]

SUMMARY

This paper proposes accurate modeling of a new high-stiffness viscoelastic material for vibration control of a structure. The temperature sensitivity of the material is probably the lowest among the viscoelastic materials available in Japan. The basic model consists of static stress element, viscoelastic element, and nonlinear viscous element. The extended model includes some modifications and an additional element to simulate stress-rise at the initial loading as well as property changes cycle-by-cycle with increased and decreased peak strain values, respectively. The extended model appears to simulate the material behavior accurately, under the random loading caused by the earthquake.

Keyword : High-stiffnes viscoelastic material, temperature dependency, frequency dependency, amplitude dependency

1. INTRODUCTION

Viscoelastic damper controls the vibration of the structure by shear deformation and corresponding energy dissipation of the viscoelastic material. In late years, significant progress has been made toward higher performance of the material [1-3], and various non-linear viscoelastic materials have been developed. During the 2011 Great East Japan Earthquake [4], response records indicated that vibrations of the buildings with velocity-dependent dampers decayed much earlier than with deformation-dependent dampers, thereby reducing number of significant cyclic deformations of the building components.

As one of the velocity-dependent dampers, the viscoelastic damper needs improvement of the material especially in regards to the following three properties: (1) reduction of temperature sensitivity for making structural design less restrictive, (2) increase in velocity-dependency for promoting vibration decay as mentioned above, and (3) increase in stiffness for making damper smaller.

Under the above points, Sumitomo Riko Company Limited ("SRK") developed a new high-stiffness viscoelastic material with reduced temperature sensitivity and larger velocity dependency, hence higher damping capacity. A styrene olefin type unique material with molecule friction, higher viscosity, and stable performance in the working temperature range is combined with the damping filler and reinforcement filler to produce the new viscoelastic material. The material has higher damping by effectively utilizing the molecule friction and viscosity, differing from the so-called high-hardness rubber that typically shows cross-linking reaction.

In order to facilitate use of this material for building vibration control, we carried out a series of experiments and have produced the large data base useful for damper and building design. The paper will discuss the data base of important dynamic properties of the material, as well as constitutive equations and numerical model for time-history analysis of buildings with the new high-performance viscoelastic dampers.

1 Sumitomo Riko Company Limited,Aichi,Japan Email：tomokazu.takada@jp.sumitomoriko.com

2 Sumitomo Riko Company Limited,Aichi,Japan Email：kaoru.yasui@jp.sumitomoriko.com

3 Sumitomo Riko Company Limited,Aichi,Japan Email：ta.nomura@jp.sumitomoriko.com

4 Prof., Struct.Eng.Res.Center,Tokyo Institute of Technology,Yokohama, Japan Email：kasai@serc.titech.ac.jp

5 Union System Company,Tokyo, Japan Email：hisao-yamazaki@unions.co.jp

2. EXPERIMENT

2.1 Experimental Scheme

As shown in Fig 1., the specimen contains the two viscoelastic layers. Each layer has thickness 5mm, width 40mm, and length 70mm. Thus total shear area of the two layers is 5,600mm^2. Test conditions are similar to those in Kasai's study [1], and are summarized as follows (Table1):

(1) Monotonic loading with constant strain rate.
(2) Sinusoidal loading with constant peak strain.
(3) Sinusoidal loading with gradually increased and decreased peak strain.
(4) Sinusoidal loading with gradually decreased and increased peak strain.
(5) Sinusoidal loading with gradually shifted and increased peak strain.
(6) Sinusoidal loading with gradually shifted and decreased peak strain.
(7) Random loading applying deformation histories of the damper in a building subjected to earthquake.

In the above loading cases, frequency and temperature are also varied as indicated in Table 1. To grasp the static behavior, each case contains what we consider the "static loading". They are 0.2%/sec strain rate for case 1, and frequency of 0.001Hz for cases 2 to 6, and 1.65%/s for case 7 (the minimum of the strain rates varying 1.65 to 855%/sec for all cycles).

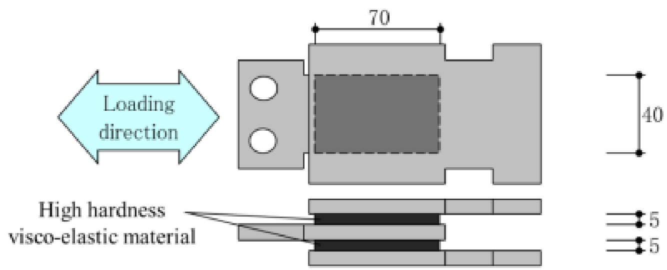

Fig.1 Test specimen

Table.1 Loading methods

No.	Loading Methods	Time Histoy	Strain rate or Strain Amplitude	Temperature・Frequency
1	Constant strain rate (monotonic)	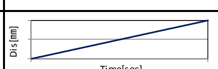	Strain rate : 0.2, 2, 20, 200 %/s	20℃
2	Constant peak strain	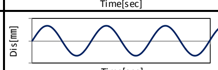	γ_{peak} : $\begin{pmatrix}+10\\-10\end{pmatrix}, \begin{pmatrix}+20\\-20\end{pmatrix}, \begin{pmatrix}+50\\-50\end{pmatrix}, \begin{pmatrix}+100\\-100\end{pmatrix}, \begin{pmatrix}+200\\-200\end{pmatrix}, \begin{pmatrix}+300\\-300\end{pmatrix}$ %	0,20,40℃ : 0.001, 0.1, 0.3, 1.0, 3.0Hz
3	Increased and decreased peak strain	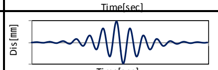	γ_{peak} : $\begin{pmatrix}+5\\-5\end{pmatrix} \sim \begin{pmatrix}+300\\-300\end{pmatrix} \sim \begin{pmatrix}+5\\-5\end{pmatrix}$ %	20℃ : 0.001, 0.1, 0.3, 1.0, 3.0Hz 0, 40℃ : 0.001Hz
4	Decreased and increased peak strain	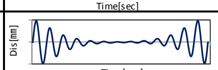	γ_{peak} : $\begin{pmatrix}+300\\-300\end{pmatrix} \sim \begin{pmatrix}+5\\-5\end{pmatrix} \sim \begin{pmatrix}+300\\-300\end{pmatrix}$ %	20℃ : 0.001, 0.1, 0.3, 1.0, 3.0Hz 0, 40℃ : 0.001Hz
5	Shifted and increased peak strain	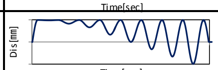	γ_{peak} : $\begin{pmatrix}+300\\+298\end{pmatrix} \sim \begin{pmatrix}+300\\-300\end{pmatrix}$ %	20℃ : 0.001, 1.0Hz
6	Shifted and decreased peak strain	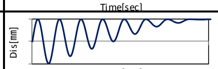	γ_{peak} : $\begin{pmatrix}+300\\-300\end{pmatrix} \sim \begin{pmatrix}+300\\+298\end{pmatrix}$ %	20℃ : 0.001, 1.0Hz
7	Earthquake response	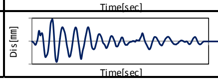	Strain amplitude random Eathquake wave : JMA Kobe, EL Centro, Taft	0,20,40℃ : 24th floor building 1st floor respond wave

2.2 Experimental results

Fig. 2 shows example results from load case 2 mentioned above, where the results from static and dynamic loading are shown by solid and broken lines, respectively. The hysteresis due to dynamic loading is much larger than due to static loading, which indicates significant velocity-dependency. In dynamic loading of peak shear strain γ =10%, the hysteresis loop is elliptical, and the equivalent stiffness is about 2.2 MPa, very stiff compared with, for instance, the typical storage stiffness of about 0.20 MPa for the acrylic polymer [2]. When peak shear strain γ =300%, the hysteresis loop is like a rectangle with pinching, and the equivalent stiffness is about 0.31 MPa, much lower than the small strain case. Figs. 2b and c show larger stiffness for higher frequency (Fig. 2b) and lower temperature (Fig. 2c), but these sensitivities are small compared to a conventional linear viscoelastic material [2]. Moreover, the similar effects of frequency and temperature suggest frequency-temperature equivalency principle would be applicable to the present material, like other materials studied by Kasai et al [1-3].

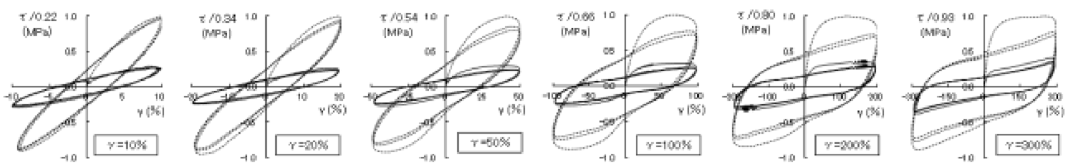

(a) Amplitude dependency (20℃,1Hz・0.001Hz)

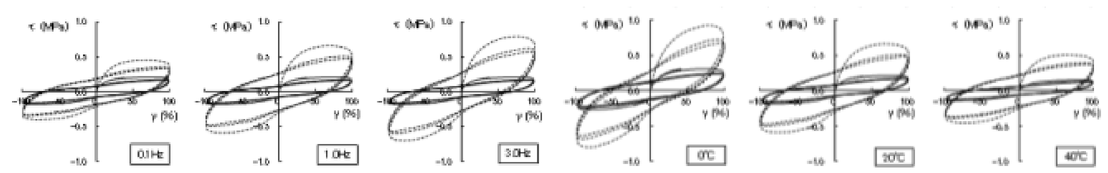

(b) Vibration frequency dependency (20℃,100％)　　　(c) Temperature dependency(100％,1Hz・0.001Hz)

Fig 2 Dependency towards amplitude, vibration frequency, and temperature of viscoelastic material （―Static Stress, ---Dynamic Stress）

3. BASIC MODEL

Based on the test results (e.g., Fig. 2), the “basic model” simulating the stable second and third hysteresis loops will be formulated. It utilizes Kasai et al.’s model [1] that were originally formulated for the high-stiffness rubber material that has more deformation dependency and less velocity-dependency than the present high-stiffness visoelastic material.

Considering three analytical elements in parallel (Fig. 3), shear stress τ of the material is considered to be the sum of the static stress τ_s , viscoelastic stress $\tau_{d,ve}$, and viscous stress $\tau_{d,vs}$, *i.e.*,

$$\tau = \tau_s + \tau_{d,ve} + \tau_{d,vs} \tag{1}$$

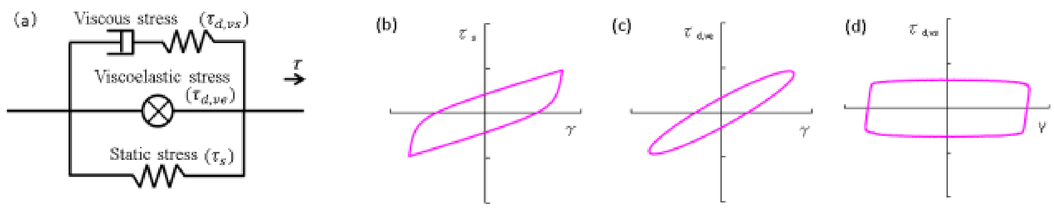

Fig. 3 Basic Model: (a) Three elements used, (b) $\tau_s - \gamma$ curve, (c) $\tau_{d,ve} - \gamma$ curve, and (d) $\tau_{d,vs}$ - γ curve

3.1 Static stress element

The static stress τ_s is calculated using the Menegotto-Pinto model [5], and the τ_s - γ curve is given by Eq. 2:

$$\tau_s = \tau_\gamma + \lambda_{\theta s}\left[G_{s2} + (G_{s1} - G_{s2})/\left\{1 + \left(\frac{\gamma - \gamma_\gamma}{\gamma_a - \gamma_\gamma}\right)^R\right\}^{1/R}\right](\gamma - \gamma_\gamma) \tag{2}$$

where τ_r and γ_r = static shear stress and shear strain at the loading reversal, G_{S1} and G_{S2} = slopes of the asymptotes, R = curvature parameter for the hysteresis loop, and $\gamma_a = \gamma_r - \tau_r / G_{S1}$, as shown by Fig. 3. For the basic model, the asymptotes are restricted to intersect at the horizontal axis (i.e., $\tau_a = 0$). The values of R, G_{S1}, and G_{S2} are estimated for the best fit to the experimental hysteresis in load cases 2 (Sec. 2.1) where $|\gamma_r|$ = 0.1, 0.2, 0.5, 1, 2, and 3 with frequency 0.001Hz. The R–value is found stable, thus, R = 0.998 is determined. Based on the values of G_{S1} and G_{S2} for different $|\gamma_r|$-values, the following relationship is obtained:

$$G_{s1} = -0.136|\gamma_{r,\max}|^2 + 0.306|\gamma_{r,max}| + 2.94\,, \qquad G_{s2} = 0.102|\gamma_{r,max}|^{-0.621} \tag{3a, b}$$

where $\gamma_{r,\max}$ is the maximum value of $|\gamma_r|$'s experienced up to the present cycle, and is obviously equal to $|\gamma_r|$ when the stabilized cycles are considered as in this chapter.

Further, by the least square method, the values of $\lambda_{\theta s}$ to match τ_s of Eq. 2 to the experimentally obtained stress are estimated for θ = 0℃ and 40℃ (Fig.6). Accordingly, Eq. 5 is obtained by setting $p = -0.0076$ and standard temperature θ_{ref} = 20℃:

$$\lambda_{\theta s} = p(\theta - \theta_{ref}) + 1 \tag{4}$$

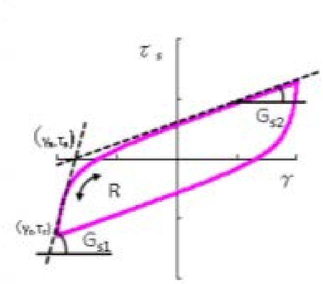

Fig. 4 Menegotto-Pinto model

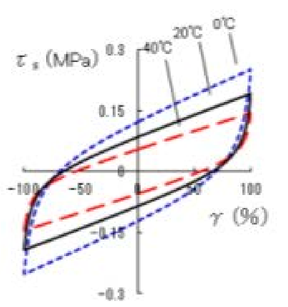

Fig 5 Temperature sensitivity of static stress component

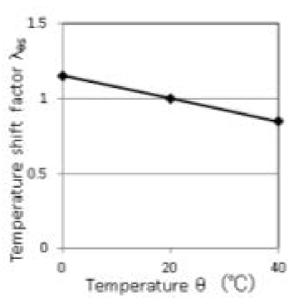

Fig 6 $\lambda_{\theta s}$ $-\theta$ relationship

Note also that by subtracting the static stress component τ_s (Eq. 2) from the experimental stress τ (Eq. 1) under the dynamic loading defined in Sec. 2.1, the dynamic stress component is obtained. It will be expressed by viscoelastic stress component $\tau_{d,ve}$ (Fig. 3c) and viscous stress component $\tau_{d,vs}$ (Fig. 3d), respectively in order to maintain accuracy over the wide range of frequencies and strain. The $\tau_{d,ve}$ - γ curve is an elliptical hysteresis loop with inclination, and $\tau_{d,vs}$ - γ curve typical nonlinear hysteresis loop, as shown earlier by Fig. 3.

3.2 Viscoelastic element

Viscoelastic stress component $\tau_{d,ve}$ (Fig. 3c) is simulated by the fractional derivative constitutive rule [2], *i.e.*,

$$\tau_{d,ve}+aD^{\beta}\tau_{d,ve}=G_d\left(\gamma+bD^{\beta}\gamma\right) \tag{5}$$

where a and b are constants depending on temperature and shear strain amplitude, as will be explained. By substituting sinusoidal strain of circular frequency ω into Eq. 5, we obtain the mathematical expressions for the storage stiffness $G'$and loss factor η as follows:

$$G'=G_d\frac{1+ab\omega^{2\beta}+(a+b)\omega^{\beta}\cos(\beta\pi/2)}{1+a^2\omega^{2\beta}+2a\omega^{\beta}\cos(\beta\pi/2)}\quad,\quad \eta=\frac{(-a+b)\omega^{\beta}\sin(\beta\pi/2)}{1+ab\omega^{2\beta}+(a+b)\omega^{\beta}\cos(\beta\pi/2)} \tag{6a,b}$$

We found equivalency among the frequency, temperature, and strain amplitude for this material. Therefore, the values of $G'$and η at arbitrary temperature θ and strain amplitude γ under the frequency ω are considered to equal those under the reference temperature θ_{ref} = 20℃, reference strain amplitude $\gamma_{ref}=2.0$, and the shifted frequency $(\lambda_{\theta d}\,\lambda_{\gamma d})\omega$, where the $\lambda_{\theta d}$ and $\lambda_{\gamma d}$ are called as the shift factors. The so-called "temperature-deformation-frequency equivalency" for the dynamic stress element is implemented to the viscoelastic stress element as follows:

By substituting $(\lambda_{\theta d}\lambda_{\gamma d})\omega$ into Eq. 6 and to obtain the same values of $G'$and η as those from Eq. 6, the values of a and b are shifted by the following:

$$a=a_{ref}\left(\lambda_{\theta d}\lambda_{\gamma d}\right)^{\beta}\ ,\qquad b=b_{ref}\left(\lambda_{\theta d}\lambda_{\gamma d}\right)^{\beta}$$

$$\lambda_{\theta d}=exp\left[\frac{-p_1\left(\theta-\theta_{ref}\right)}{\left(p_2+\theta-\theta_{ref}\right)}\right]\quad,\quad \lambda_{\gamma d}=exp\left[\frac{-p_3\left(\gamma_{r,max}-\gamma_{ref}\right)}{\left(p_4+\gamma_{r,max}-\gamma_{ref}\right)}\right] \tag{7a-d}$$

In the similar manner as for high-stiffness rubber [1], the least square method is used to best simulate $G'$and η at θ_{ref} and γ_{ref} mentioned above. Accordingly, G_d =0.00008MPa, a_{ref} =0.0136, b_{ref} =1013, and β=0.238.

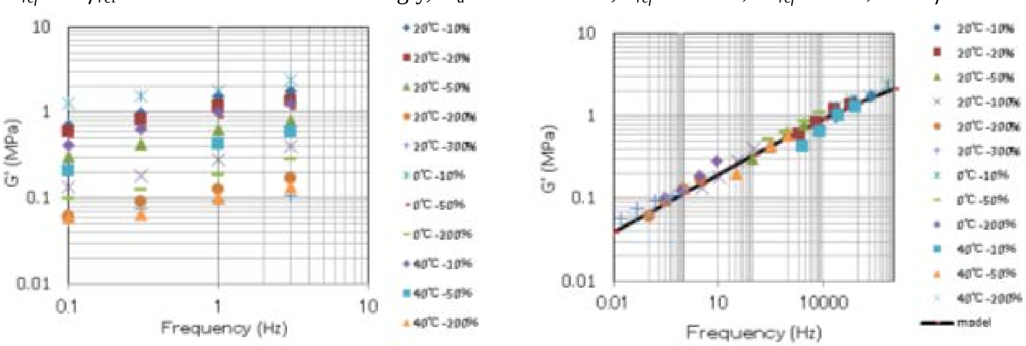

(a) G' obtained from experiment (b) G' plotted by using shift factor

Fig. 7 Temperature- and deformation-dependencies of the high-stiffness viscoelastic material

Further, for the arbitrary θ from 0 to 40℃, and strain amplitude γ_r from 0.1 to 3.0, the curves in Fig.7a are shifted to that in Fig. 7b, and necessary values of p_1,p_2,p_3,and p_4= -55164742, -1045454914, 7.832, and 3.229, respectively, are obtained by the least square method. Note that the properties of the element are adjusted by the initial temperature θ and the corresponding $\lambda_{\theta d}$ value, as well as the strain amplitude γ_r and corresponding $\lambda_{\gamma d}$ value reset at each load reversal.

3.3 Viscous element

Viscous stress component $\tau_{d,vs}$ (Fig. 3d) is simulated by the Maxwell model combining in series the elastic element and viscous element producing the force proportional to fractional power α of strain velocity, i.e.,

$$\dot{\gamma} = \frac{\tau_{d,vs}}{q_1 K_d} + \left(\frac{|\tau_{d,vs}|}{q_1 C_d}\right)^{\frac{1}{\alpha}} \cdot \frac{sgn(\tau_{d,vs})}{\lambda_{\theta d}\lambda_{\gamma d}} \quad (8)$$

where C_d and K_d are viscosity coefficient of the viscous element and stiffness of the elastic element, respectively. The value of $\tau_{d,vs}$ for the given γ is obtained by numerical integration of Eq. 8. The dependency of the Maxwell model on the value of the strain γ_r at each load reversal is simulated by multiplying q_1 to both C_d and K_d . Also, q_1 is set to 1.0 for the stable cyclic loading with γ_r = 2.0, and α, C_d and K_d are determined by the least square method. The Maxwell model shows the stiffness close to that of the elastic element q_1K_d at small strain or at the beginning of loading/unloading, and the stiffness of the elastic element is set to q_1K_d where K_d=1 MPa.

Accordingly, K_d=1 MPa, C_d=0.137 MPa·s$^{0.154}$ and α = 0.154 are obtained at θ_{ref} = 20℃, γ_{ref} =2.0, and frequency 0.3Hz. By fixing these values, the values of q_1 are obtained for different γ_r's by the least square method, and they are curve-fitted as follows:

$$q_1 = 0.0286|\gamma_{r,max}|^2 + 0.456|\gamma_{r,max}| - 0.0242 \qquad (q_1 \geq 0) \quad (9)$$

4 EXTENDED MODEL

In this section, the basic model simulating the stabilized cycles of constant peak strain (Sec. 3) is extended to model the first cycle as well as subsequent cycles with varied peak strains.

4.1 Modeling for the First Loading

The hysteresis at the first cycle differs from those at the subsequent cycles, and the three elements (Fig. 3a) are used as they are except that the values of the parameters are modified accordingly. The parameter values determined in Sec. 3.1 for the stabilized cyclic loading of the static stress element is now changed by considering very slow monotonic loading (loading case 1, Sec. 2.1). The Menegotto-Pinto model in Fig. 4 is used but by changing the parameter values such that G_{S1} = 0.67 MPa, G_{S2} = 0.082 MPa, and τ_a =0.175 MPa in Eq. 2, where γ_r= τ_r = 0 is considered.

For the viscoelastic element (Sec. 3.2), the γ_r in Eq. 7d is replaced by the present value $|\gamma|$ which is updated step-by-step from the initial zero value until the load reversal. Accordingly, the larger value of the shift factor $\lambda_{\gamma d}$, hence larger stiffness of the element is used at the initial loading.

For the viscous and elastic elements of the Maxwell model (Sec. 3.3), no changes are made. However, another viscous element is connected in parallel with the three elements, and adds the stress $\tau'_{d,vs}$ until the first loading reversal. The element shows quick stress-rise, depending on the temperature as follows:

$$\tau'_{d,vs} = \gamma C'_d(\lambda'_{\theta d}|\dot{\gamma}|)^{\alpha'}, \quad \lambda'_{\theta d} = p'_1\, exp(p'_2\theta) \quad (10a,b)$$

where C'_d=0.00613 Mpa·s$^{0.6}$, α' = 0.6, p'_1 = 11.7, and p'_2 = −0.121.

After the first load reversal, the parameters of the static stress element are reset to those of the basic model (Chap. 3), and the added viscous element is made inactive. Good accuracy for various cyclic loading cases will be demonstrated in Chap. 5.

4.2 Sinusoidal Cyclic Loading with Increased or Decreased Peak Strain

For the cyclically applied strains with varying peak magnitudes, the model is adjusted depending on whether the $|\gamma_r|$ at the present cycle is larger than $\gamma_{r,\max}$ or not. When $|\gamma_r| > \gamma_{r,\max}$, the case is called the "*peak strain increasing case*", and is otherwise called "*peak strain decreasing case*". From now, we use $\gamma_{r,i}$ as the value of the strain at i-th load reversal. Fig. 8a shows the general cyclic loading case with the load reversal numbers i-1, i, i+1 ($i \geq 3$), and Fig. 8b shows the initial loading and subsequent cycles with the load reversal 1 and 2. The following describes the modeling for the two cases, respectively:

4.2.1 Static Stress Element

Peak strain increasing case : The γ-τ_s curve after load reversal i (Fig. 8a) or load reversal 1 (Fig. 8b) corresponds to the peak strain increasing case which does not require adjustment. They are obtained from Eq. 1, where G_{S1} and G_{S2} are determined by substituting the value of $\gamma_{r,i}$ (Fig. 8a) or $\gamma_{r,1}$ (Fig. 8b) into Eqs. 3 and 4, respectively.

Peak strain decreasing case A (Fig. 8a): The γ-τ_s curve after load reversal i+1 corresponds to the peak strain decreasing case A, since $|\gamma_{r,i+1}| < \gamma_{r,\max}$. As the preliminary, draw the bounding curve by extending the portion from $\gamma = \gamma_{r,i}$ to $-\gamma_{r,i}$, as if the load reversal at $\gamma_{r,i+1}$ did not occur, and from $\gamma = -\gamma_{r,i}$ to $\gamma = \gamma_{r,i}$ (broken line in Fig. 8a). After these, the γ-τ_s curve starting from ($\gamma_{r,i+1}$, $\tau_{r,i+1}$) is expressed by Eq. 1 where G_{S1} is determined by substituting the value of $\gamma_{r,i+1}$ into Eq. 3, and G_{S2} is determined as the slope between ($\gamma_{a,i+1}$, 0) and ($\gamma_{r,i}$,$\tau_{r,i}$) as shown by Fig. 8a. Note that $\gamma_{a,i+1} = \gamma_{r,i+1} - \tau_{r,i+1}/G_{S1}$. If the curve intersects with the bounding curve, it is superseded by the bounding curve (Fig. 8a).

Peak strain decreasing case B (Fig. 8b): The γ-τ_s curve after load reversal 2 corresponds to the peak strain decreasing case B, since $|\gamma_{r,2}| < \gamma_{r,\max}$ (=$|\gamma_{r,1}|$). In a similar manner as in Fig. 8a, draw a curve by extending the portion from $\gamma = \gamma_{r,1}$ to $-\gamma_{r,1}$, as if the load reversal at $\gamma_{r,2}$ did not occur, and from $\gamma = -\gamma_{r,1}$ to $\gamma = \gamma_{r,2}$ (broken line in Fig. 8b). The coordinate of the end point is expressed as ($\gamma_{r,1}$, τ_r'). After these, the γ-τ_s curve starting from ($\gamma_{r,2}$, $\tau_{r,2}$) is expressed by Eq. 1 where G_{S1} is determined by substituting the value of $\gamma_{r,2}$ into Eq. 3, and G_{S2} is determined as the slope between ($\gamma_{a,2}$, 0) and ($\gamma_{r,1}$, τ_r'), see Fig. 8b. Note that $\gamma_{a,2} = \gamma_{r,2} - \tau_{r,2}/G_{S1}$. If the curve intersects with the extended portion of the initial monotonic γ-τ_s curve, it is superseded by the curve (Fig. 8b).

The main difference between the peak strain decreasing cases A and B is that the former considers ($\gamma_{r,i}$,$\tau_{r,i}$), and the latter uses ($\gamma_{r,1}$, τ_r') as the constraint for the slope G_{S2}. The former also considers a full cycle of bounding curve and the latter the initial monotonic curve, respectively.

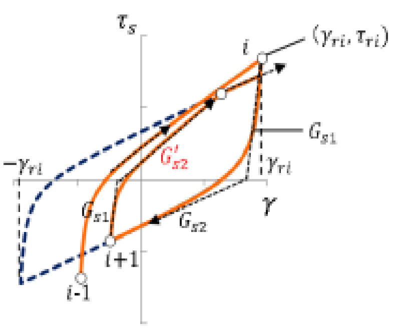

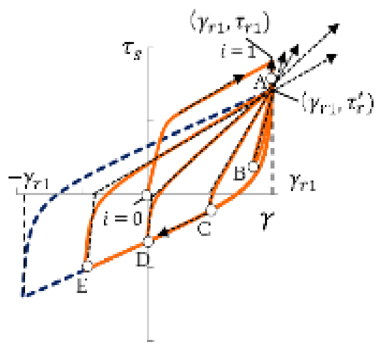

Fig. 8 Peak Strain Increasing and Decreasing Cases Involving (a) Cycles i-1, i, and i+1, and (b) Cycles 1 and 2

4.2.2 Dynamic Stress Element

Peak strain increasing case: For the viscoelastic element (Sec. 3.2), the γ-$\tau_{d,ve}$ curve for the peak strain increasing case is obtained from Eq. 7 with no adjustment. As for the viscous element (Sec. 3.3), the γ-$\tau_{d,ve}$ curve is obtained in a similar manner by updating the $\gamma_{r,\max}$ and used in Eqs. 8 and 9.

Peak strain decreasing case: For the viscoelastic element, the γ-$\tau_{d,ve}$ curve for the peak strain decreasing case is obtained from Eq. 7 with no adjustment. As for the viscous element (Sec. 3.3), the $\lambda_{\gamma d}$ (Eq. 7) is estimated differently from that for the viscoelastic element. When determining $\lambda_{\gamma d}$ in Eq. 7d and q_1 in Eq. 9, after load reversal i+1(Fig. 8a) or load reversal 2 (Fig. 8b), the $\gamma_{r,\max}$ should be changed to either $\{\gamma_{r,\max}+|\gamma_{r,i+1}|\}/2$ and $\{\gamma_{r,\max}+|\gamma_{r,2}|\}/2$, respectively. This is because the hysteresis of the viscous element becomes too large, if $\gamma_{r,\max}$ is used for the peak strain decreasing case.

5 VALIDATIONS OF THE MODEL

5.1 Monotonic Loading

Fig. 9 shows the accuracy of the model for Load Case 1 in Table 1, where the τ_s - γ curve of the element agrees with the curve from the test for each of strain rates varying widely from 0.002 to 2.00/s. The extended model combining the three elements and an added element to (Eq. 10) works well. For the slowest rate, the static stress element mostly governs the curve.

Note also that it also appears to be effective for the first cycle of the cyclic loading, where the strain is applied as the sinusoidal wave and the strain rate is not constant but varies as cosine function of time. This can be seen from the later Figures 10, 13, and 14.

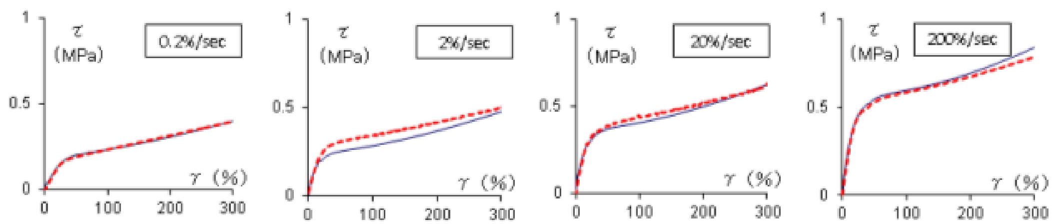

Fig. 9 Case 1: Monotonic Loading（—Experiment, ---Model）

5.2 Cyclic Loading with Constant Peak Amplitude

Fig. 10 shows the accuracy of the model for the Load Case 2 in Table 1, where three cycles of the constant peak strain are applied to the specimen. It covers the broad range of temperature 0 to 40℃, frequency 0.001 to 3.0 Hz, and shear strain amplitude of 1.0. Note that other cases of shear strain amplitudes 0.1, 0.2, 0.5, 2.0, and 3.0 were also tested (Table 1), but are not shown due to the space limitation. The analytical model appears to agree with the test, for the initial cycle as well as stable later cycles, except for the later part of the first cycle.

The temperature sensitivity of the material seen from Fig. 10 appears to be very small. As a matter of fact, it is the most insensitive among many viscoelastic materials available in Japan. Its unloading stiffness is high compared with most viscoelastic materials, enabling good deformation control as well as energy dissipation, as introduce in Chapter 1. Although not shown, the material shows can sustain the cyclic shear strains of at least ±

3.0 with no damage.

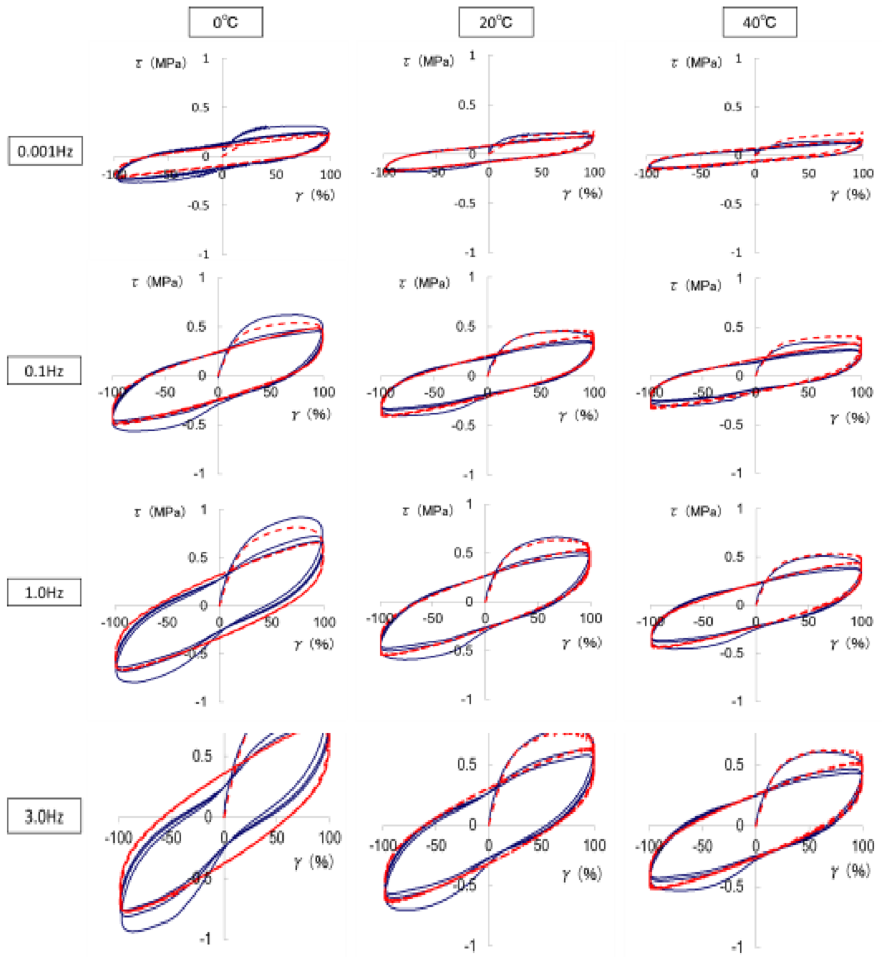

Fig. 10 Case 2: Cyclic Loading with Constant Peak Strain (—Experiment, ---Analysis)

5.3 Cyclic Loading with Increased/Decreased or Decreased/Increased Peak Strain

Fig. 11 shows the accuracy of the model for the Load Case 3 in Table 1, where cycles of increased peak strain are applied earlier (Fig. 11a), and those of decreased peak strain are applied later (Fig. 11b) to the specimen. The cycles in the earlier part are simulated mostly by the basic formulations discussed in Chap. 3 and Sec. 4.2. Those in the later part are simulated by the special formulations/algorithm explained in detail in Sec. 4.2. The model is reasonably accurate in both Figs. 11a and b for frequencies 0.1, 1.0, and 3Hz.

Fig. 12 shows the accuracy of the model for the Load Case 4 in Table 1, where cycles of decreased peak strain are applied earlier (Fig. 12a), and those of increased peak strain are applied later (Fig. 12b) to the specimen. In Fig. 12a, the cycles in the earlier part are well simulated by the special formulations/algorithm explained in detail in both Secs. 4.1 and 4.2, where the γ-τ curve of initial and subsequent cycles differ significantly from those of both Figs. 11a and b. Also, in Fig. 12b, the cycles with increased peak strain in the later part are also well simulated, and the γ-τ curve of initial and subsequent cycles differ significantly from those of Figs. 11a and b, as well as Fig. 12a. The model is reasonably accurate for frequencies 0.1, 1.0, and 3Hz.

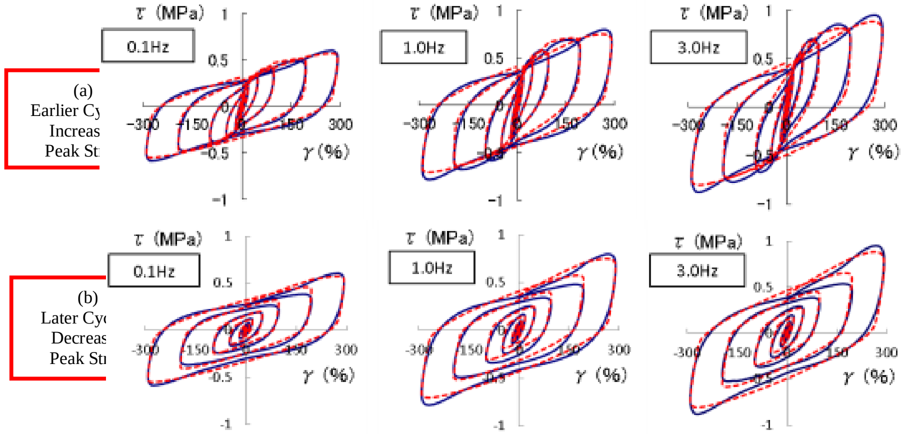

Fig. 11 Case 3: Cyclic Loading with Increased and Decreased Peak Strains（—Experiment, --- Model）

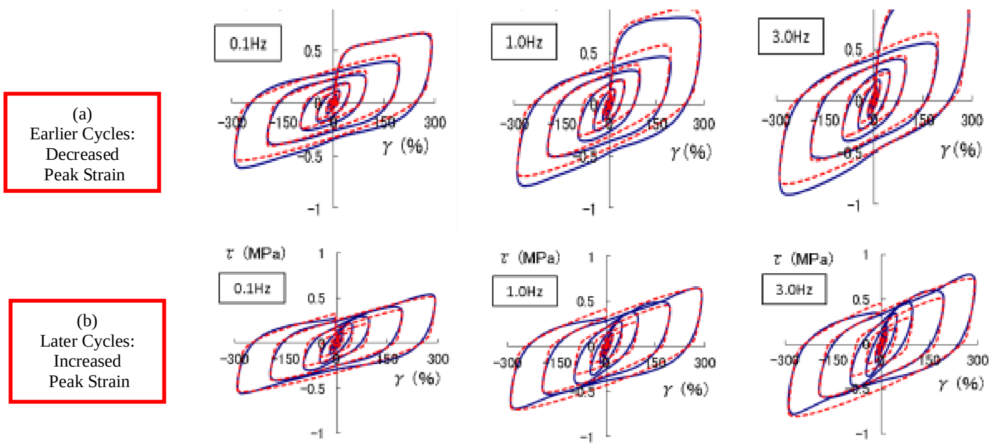

Fig. 12 Case 4: Cyclic Loading with Decreased and Increased Peak Strains（—Experiment, --- Model）

5.4 Cyclic Loading with Increased/Decreased or Decreased/Increased Peak Strain

Fig. 11 shows the accuracy of the model for the Load Case 3 in Table 1, where cycles of increased peak strain are applied earlier (Fig. 11a), and those of decreased peak strain are applied later (Fig. 11b) to the specimen. The cycles in the earlier part are simulated mostly by the basic formulations discussed in Chap. 3 and Sec. 4.2. Those in the later part are simulated by the special formulations/algorithm explained in detail in Sec. 4.2. The model is reasonably accurate in both Figs. 11a and b for frequencies 0.1, 1.0, and 3Hz.

Fig. 12 shows the accuracy of the model for the Load Case 4 in Table 1, where cycles of decreased peak strain are applied earlier (Fig. 12a), and those of increased peak strain are applied later (Fig. 12b) to the specimen. In Fig. 12a, the cycles in the earlier part are well simulated by the special formulations/algorithm explained in detail in both Secs. 4.1 and 4.2, where the γ-τ curve of initial and subsequent cycles differ significantly from those of both Figs. 11a and b. Also, in Fig. 12b, the cycles with increased peak strain in the later part are also well simulated, and the γ-τ curve of initial and subsequent cycles differ significantly from those of Figs. 11a and b, as well as Fig. 12a. The model is reasonably accurate for frequencies 0.1, 1.0, and 3Hz.

5.5 Cyclic Loading with Shifted and Either Increased or Decreased Peak Strain

Fig. 13 shows the accuracy of the model for the Load Cases 5 and 6 in Table 1. Load Case 5 applies the largest positive peak strain first, followed at the shifted position by the subsequent cycles with increased negative peak strain while keeping the positive peak strain constant. The algorithm discussed using Fig. 8b in Sec. 4.2 becomes in effect in this load case, and the analysis simulates well the test results.

On the other hand, Load Case 6 applies the largest positive and negative peak strains first, followed by the subsequent cycles with decreased negative peak strain while keeping the positive peak strain constant, thus, ends the loading at the positive shifted position. The algorithm discussed using Fig. 8a in Sec. 4.2 becomes in effect in this load case, and the analysis simulates well the test results.

Con formato: Fuente: Times New Roman, 11 pto

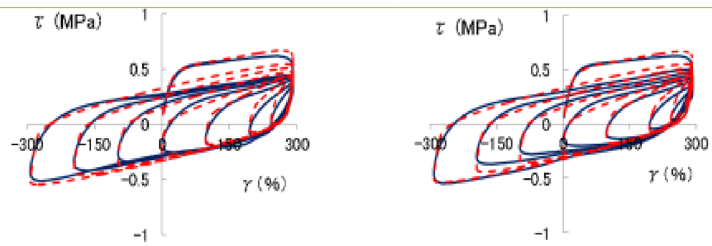

(a) Shifted and Increased Negative Peak Strain

(b) Shifted and Decreased Negative Peak Strain

Fig 13 Cases 5 and 6: Cyclic Loading with Shifted and Increased or Decreased Peak Strains
(—Experiment, --- Model)

5.6 Random Loading by Simulating Responses of Damper in Building

Fig. 14 shows the accuracy of the model for the Load Case 7 in Table 1. The strain time-histories of the damper in a building subjected to three earthquakes are used as input for the specimen and analysis model. The earthquakes considered are JMA Kobe motion, El Centro motion, and Taft motion, respectively. Since the model simulated the Load Cases 1 to 6 with reasonable accuracy, its good accuracy for the earthquake loading cases is recognizable from Fig. 14.

6 CONCLUSIONS

This paper has proposed accurate modeling of a new high-stiffness viscoelastic material for dampers against earthquakes. The model consists of static stress element, viscoelastic element, and nonlinear Maxwell element, with modifications to simulate stress-rise at the initial loading as well as property changes cycle-by-cycle with increased and decreased peak strains, respectively. The model appears to simulate the random response caused by earthquakes.

7 REFERENCES

[1] Kasai, K., Nishizawa, K., Ooki,Y., Tanaka,Y., Tanaka,K., Nishimoto.K., and Yamazaki,H. ”Static/dynamic Tests of High-hardness Rubber for Response Control and Its Time History Analysis Method”, Journal of Structural and Construction Engineering (Transactions of AIJ),2011;no.662:785-794.(in Japanese)

[2] Kasai, K., Teramoto,M.,Okuma,K.,and Tokoro,K.”Constitutive Rule for Viscoelastic Materials Considering Temperature,Freqency,and Strain Sensitiveties”, Journal of Structural and Construction Engineering(Transactions of AIJ),2001;no.543:77-86.(in Japanese)

[3] Kasai,K., Ooki,Y., Amemiya,K., and Kimura,K.”A Constitutive Rule for Viscoelastic Materials Combining Iso-Butylene and Stylene Polymers” Journal of Structural and Construction Engineering(Transactions of AIJ),2003;no.569:47-54.(in Japanese)

[4] Kasai,K.,Matsuda,K.,Chimamphant, S.”Seicmic Protection of New and Existing Super-Tall Building:Part2 Response Data Analysis and Performance Evaluations”,SEFC 2015 PROCEEDINGS

[5] Kasai,K.,Yamazaki,H.Kozawa,H.,Kaneko,H.,Sadasue,K.,and Ono,Y.”Curved Hysteresis Model of Structural Steel under Cyclic Loading : Part 7 Substantially Improved Analysis Mode”, Summaries of technical papers of Annual Meeting(AIJ),2008,907-908

Con formato: Fuente: Times New Roman, 11 pto

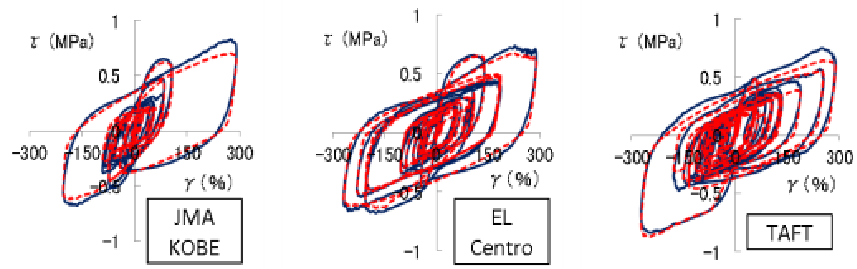

(a) Responses for Whole Duration of Seismic Loading

Con formato: Fuente: Times New Roman, 11 pto

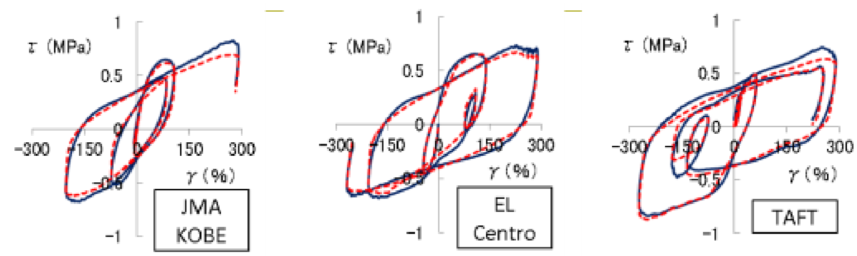

(b) Earlier Part of Responses

Con formato: Fuente: Times New Roman, 11 pto

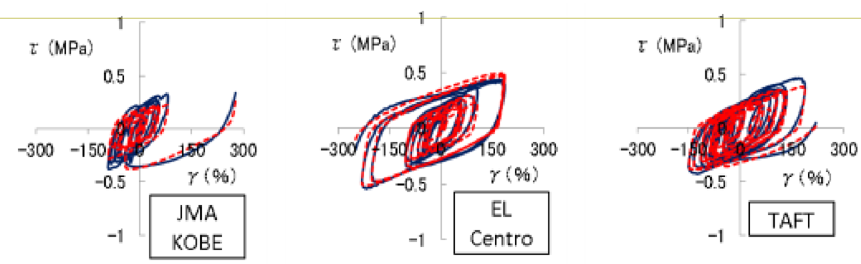

(c) Later Part of Responses

Fig. 14 Comparing experiment value and mechanical value（—Experiment, ---Mechanical）